Estimation of Temperature Profiles using Low-Frequency Distributed Acoustic Sensing from In-Well Measurements

N. A. Bradley*, NTNU; **K. E. Haavik,** Equinor ASA; and **M. Landrø,** NTNU

*Corresponding author; email: NBRAD@equinor.com

Keywords: Low frequency Distributed Acoustic Sensing; Distributed Temperature Sensing; Temperature; Downhole Monitoring

Summary

Distributed fibre-optic sensing for in-well measurements is primarily used for monitoring purposes. Distributed acoustic sensing (DAS) is used to record acoustic disturbances and is sensitive to changes in strain, pressure, and temperature. Distributed temperature sensing (DTS) is used to measure temperature along the fibre. Here, we compare temperature changes measured by DAS and DTS in wells over different time periods. We affirm the linear dependency between DAS's phase change and temperature, with the derived strain rate being proportional to the time derivative of the temperature response. Given that low-frequency (LF) DAS is sensitive to strain, pressure, and temperature effects, one must choose quiet periods in the well or condition the data to only analyse the effect of temperature on the fibre. We show that LF-DAS data can be used to track temperature changes over several weeks.

We then propose a method, using liquid column movements, to invert LF-DAS data for absolute temperature profiles. The temperature profile in a well can be measured using DTS. However, DTS data is not always available, and conventional Raman scattering DTS is not used in subsea wells with long lead-in lengths. Hence, it would be desirable to acquire the temperature response from LF-DAS data to use as a multipurpose tool for in-well monitoring. Here we show that when purely investigating the response to an initial displacement of the fluid column, i.e., from rest, LF-DAS can be used along with reference sensors, such as the wellhead and downhole temperature gauge data to estimate the depth variations in temperature in production and injection wells.

Introduction

The emergence of fibre-optic cables towards active monitoring allows for the recording of acoustic energy along extensive lengths of optical fibre deployed along the wellbore, capturing amplitude and phase information over a wide frequency and high dynamic range (Xiao et al. 2014). Preliminary research determined that Distributed Acoustic Sensing (DAS) could be used to detect the acoustic field in a variety of wells with Johannessen et al. (2012) highlighting the value of delivering well and reservoir data along the entire length of the well towards optimising production.

DAS systems are sensitive to changes in temperature. These variations can be monitored during a variety of operational processes including hydraulic fracture monitoring (Bakku et al., 2014; Karrenbach et al., 2017), microseismic event detection (Metsayer et al., 2011; Webster et al., 2013), production/injection profiling (Horst et al. 2015), well integrity monitoring (Raab et al. 2019), gas-lift optimization (Koelman et al. 2012), geomechanical modelling (Sherman et al. 2019) and recording of multiphase flow measurements (Fidaner et al. 2017). Distributed Temperature Sensing (DTS) systems are also commonly deployed in wells, as to which the measurements are similarly affected by variations in temperature. Applications include monitoring for wellbore leakage

(Mao et al. 2017), well treatment (Sharma et al. 2010), fractures (Wang and Bussear, 2011; Malanya et al., 2016), reservoir characterisation (Leone et al. 2015), and flow and injection profiling (Kabir et al., 2008; Foo et al., 2014).

Temperature changes observed in wells can be gradual over larger time scales such as monitoring warm-back periods or more discrete at smaller scales such as monitoring temperature variation due to changes in production/injection flow rate. The signals associated with temperature-related events can be observed in low-frequency (LF) DAS data. However, LF-DAS is not only sensitive to temperature variations, but also pressure acting on the fibre-optic cable and pressure-induced strain (Haavik, 2022). For example, fluid flow giving rise to strain or pressure acting on steel surfaces inducing tubing strain. Consequently, using LF-DAS as a temperature sensor requires extensive conditioning of the data, including signal processing and denoising techniques to isolate the temperature response.

Limitations of Raman-Based DTS. The DTS data acquisition setup simulates an array of temperature sensors along the entire length of the fibre (Johnson et al. 2016). The technique relies on Raman-based scattering and is sensitive to changes in temperature. DTS measurements are acquired by firing a laser pulse down the fibre, with the Raman band of the back-scattered light being used to estimate the temperature. Frequency shifts associated with the Raman band are known as the stokes and anti-stokes components of the backscatter spectra (Cannon and Aminzadeh 2013). Since the fibre itself is sensitive to temperature, the ratio of amplitudes of stokes and anti-stokes backscatters can be correlated with temperature (Farahani et al. 1999):

$$\boldsymbol{T(z,t)} = \frac{\boldsymbol{\gamma}}{\boldsymbol{\ln(R(z,t)) + C(t) - \int_0^z \Delta\alpha(z')dz'}} \qquad (1)$$

where $\boldsymbol{T(z,t)}$ is the temperature at a distance along the fibre ($\boldsymbol{z}$) at a given time ($\boldsymbol{t}$), $\boldsymbol{\gamma}$ represents the energy shift between a photon at the incident laser wavelength and scattered Raman wavelength, $\boldsymbol{R}$ is the ratio between stokes and anti-stokes amplitudes, $\boldsymbol{C}$ is a calibration parameter linked to offset from vibrations and thermal effects and $\boldsymbol{\Delta\alpha}$ is the differential attenuation of the backscattered stokes and anti-stokes (Soroush et al. 2021).

The signal-to-noise ratio of DTS systems is fundamentally limited by two main effects. Firstly, the energy input into the fibre is primarily constrained by Simulated Raman Scattering (SRS), which is a non-linear effect. This occurs because the wavelength of the Raman-scattered light differs from that of the incident light, thereby restricting the amount of power that can be launched as a probe (Hartog, 2017). Secondly, there is a correlation with the wavelength dependence of the measured stoke and anti-stoke intensities. It is worth noting that the Brillouin band of scattering, which is sensitive to strain and temperature, can be utilised to overcome the challenges associated with Raman-based DTS acquisition.

These limitations have a major impact when used in subsea wells with long lead-in lengths due to attenuation of optical connections, splices, and downhole fibres (Seabrook et al. 2022). In addition, the number of fibre-optic cables is limited at the subsea tree with older versions of optical feedthrough systems being limited to a single fibre (Shiach et al., 2007). In the deployment of subsea wells, it is common for the well to pass through a manifold, making them highly extensive in length. When using longer fibre lengths, the effect of attenuation suffered by probe and Stokes pulses must be considered as a major limiting factor (Smith, 1972). Thus, in the context of long lead-in subsea wells, DTS systems are less practical due to the increased noise encountered when the distance from the source is extended, with Raman scattering being more susceptible to noise. To overcome this limitation, maturing fibre optic technology such as optical circulators can be placed at the subsea tree reflections (Wilson et al. 2022), limiting the sensing portion of the fibre to eliminate undesirable backscatters. However, to avoid the cost of such novel tools, DAS systems (which are

commonly deployed in conjunction with DTS) can be utilised as an alternative approach to measure temperature changes, allowing for interrogation of over 100km in fibre length (Bouffaut et al. 2022).

Temperature Dependency of DAS. The DAS method utilises a fibre-optic interrogator unit to measure the dynamics of a strain field acting on a fibre, sending and receiving coherent laser light pulses to and from the fibre that it is attached to (Lindsey et al. 2020). When strain acts on a cable, it is elongated or compressed leading to a change in the optical phase. This information can be used in conjunction with the speed of light within the cable to assess the location and amount of strain on the cable. The output of the data is the change in optical phase (Budiansky et al. 1979):

$$\Delta\boldsymbol{\phi} = \boldsymbol{\phi}\left(\frac{\Delta \boldsymbol{L}}{\boldsymbol{L}} + \frac{\Delta \boldsymbol{n}}{\boldsymbol{n}}\right) \quad (2)$$

where $\boldsymbol{\phi}$ is the optical phase, $\frac{\Delta \boldsymbol{L}}{\boldsymbol{L}}$ is the axial strain in the fibre and $\frac{\Delta \boldsymbol{n}}{\boldsymbol{n}}$ represents the relative change of refractive index in the fibre. The resultant change in optical phase is sensitive to changes in strain and temperature.

The sensitivity of DAS to temperature changes can be attributed to two main factors: thermal expansion; and the thermal optic effect. Thus, the change in optical phase with respect to temperature effects can be expressed as (Fang et al. 2012):

$$\Delta\boldsymbol{\phi} = \boldsymbol{\phi}\Delta\boldsymbol{T}(\boldsymbol{\alpha_T} + \boldsymbol{\xi}) \quad (3)$$

where $\Delta\boldsymbol{T}$ is the change in temperature, $\boldsymbol{\alpha_T} = \frac{\boldsymbol{1}}{\boldsymbol{L}}\frac{\boldsymbol{dL}}{\boldsymbol{dT}}$ is the thermal expansion coefficient and $\boldsymbol{\xi} = \frac{\boldsymbol{1}}{\boldsymbol{n}}\frac{\boldsymbol{dn}}{\boldsymbol{dT}}$ is the thermal optic effect coefficient. The typical values of these terms for a silica fibre are $\boldsymbol{0.5 \times 10^{-6} K^{-1}}$ (Roy et al. 1989) and $\boldsymbol{1 \times 10^{-5} K^{-1}}$ (Gao et al. 2018), respectively.

Traditionally, DTS has been used as the primary tool for observing temperature variation using fibre-optic sensing. However, as described above, subsea wells with long lead-in lengths (>10km) suffer from optical loss mainly due to connections and splices, which makes DTS measurements less than desirable for this specific application. Thus, it would be beneficial to use DAS in conjunction with other temperature sensors to allow for the extraction of information during or directly after in-well procedures. The main motivation behind this study is to acquire the absolute temperature response from LF-DAS data and apply this in the context of temperature profiling.

Karrenbach et al. (2019) and Legget et al. (2023) utilise the linear dependence of the LF-DAS response to temperature changes to estimate temperature-compensated strain using LF-DAS and DTS data. Sidenko et al. (2022) shows the effect of temperature for in-well DAS measurements, obtaining constants to convert strain readings to temperature for a variety of cable types and acquisition setups. This paper aims to extend these results, affirming that the DAS response is proportional to the time derivative of temperature, alongside showing that LF-DAS is sufficient to capture temperature variation over longer time periods (several weeks). This is shown under the heading “Scaling of LF-DAS to Temperature-gradient”, using data from a well without a long lead-in, so that DTS data is available to validate the approach. Lauber and Lees (2021) show that merging of the temperature response of DTS and DAS data leads to improved temperature resolution and more accurate absolute temperature results. Jin et al. (2019) determines the statistical distribution of total fluid production by combining DTS, measuring the temperature during steady state conditions, with DAS, measuring flow velocity by tracking temperature slugs during the transient state. We show that incorporating reference temperature information from either DTS or temperature gauge information will allow for measurement of absolute temperature variation over time. Here, we also suggest a method for estimating the absolute temperature profile along the fibre based

on LF-DAS calibrated to two-gauge measurements. Knowledge of temperature trends from producing or injecting wells can be useful, for example, in monitoring changes in the overburden by tracking temperature variation due to out of zone injection.

Fibre Optic System

The streaming solution for DAS and DTS data consists of three main parts (Schuberth et al. 2021). First, fibre-optic interrogators offshore are streaming raw DAS and DTS data via a dedicated cable to shore, the fibre optic cables are clamped to the production tubing. Next, a high-performance computing processing cluster transforms and decimates the data to make it manageable for live streaming. Finally, the decimated data is streamed to a custom-made cloud-based visualization platform, allowing for real-time monitoring of DAS and DTS data.

Scaling of LF-DAS to Temperature-gradient

To capture the effect of temperature on LF-DAS data, signal processing is required to remove any effects from strain and/or pressure. An approach for mitigating these undesirable effects from strain and pressure is to choose a time where the well is essentially standing still (no operations). It is worth noting that even if the well is under static conditions, pressure differences between zones could lead to fluid migration (cross-flow) through the wellbore. However, such variations would be particularly visible in the LF-DAS data. Ultimately, a period was chosen during which we have approximately three weeks of data. This period corresponds to the well experiencing a warm-back effect after a loss of liquids during completion, gradually heating back up towards the geothermal temperature. As is observed in **Fig. 1** (DTS) and **Fig. 2** (LF-DAS), the warm-back effect is visible between depths 3885 - 3925m. This heating up is observed in both the DTS and LF-DAS data. Here, the LF-DAS data has much higher resolution in time than the DTS with sampling intervals of 0.8s and 5min, respectively. The DTS data acquired for this study utilises a DTS box that cycles between different wells, sampling a total of 8 wells. It samples a well every minute, estimating the average signal over that interval, and then switches to the next well. Thus, the lower sampling in DTS is simply a consequence of the data acquisition setup.

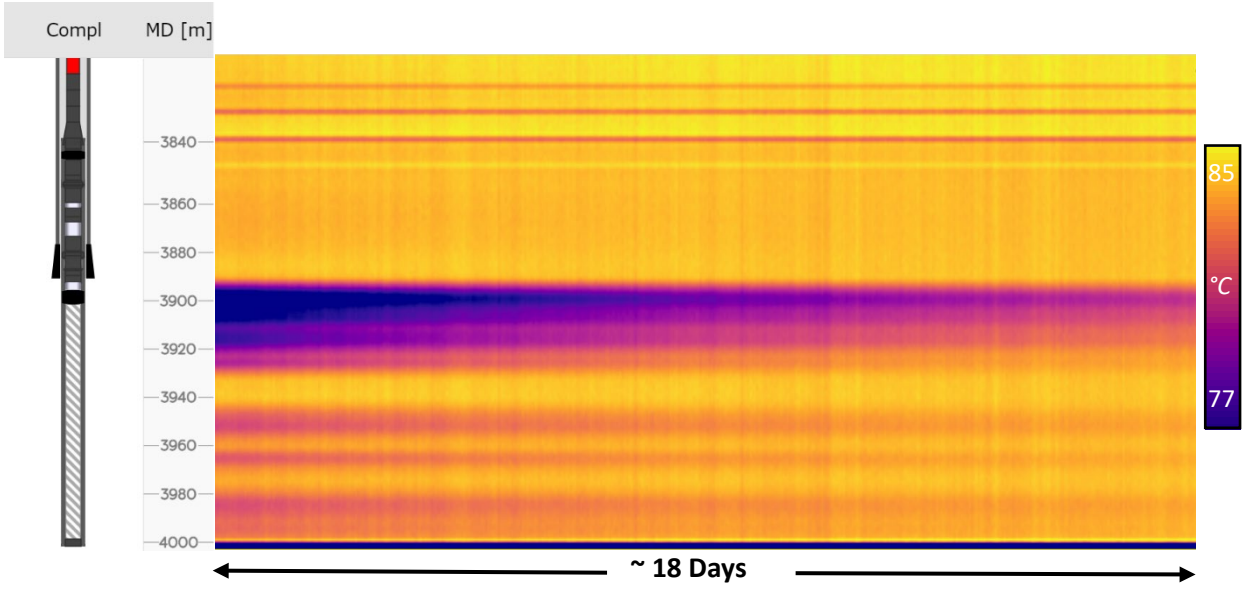

Figure 1: DTS data (temperature traces) from an injection well which has not started injection. Display shows a warm-back period of around three weeks, heating up to original temperatures after a loss of liquids during completion of the well (largest temperature change across the full length of the profile is ~4°C). The horizontal axis corresponds to increasing time from left to right and the vertical axis represents the measured depth below rotary kelly bushing (mRKB).

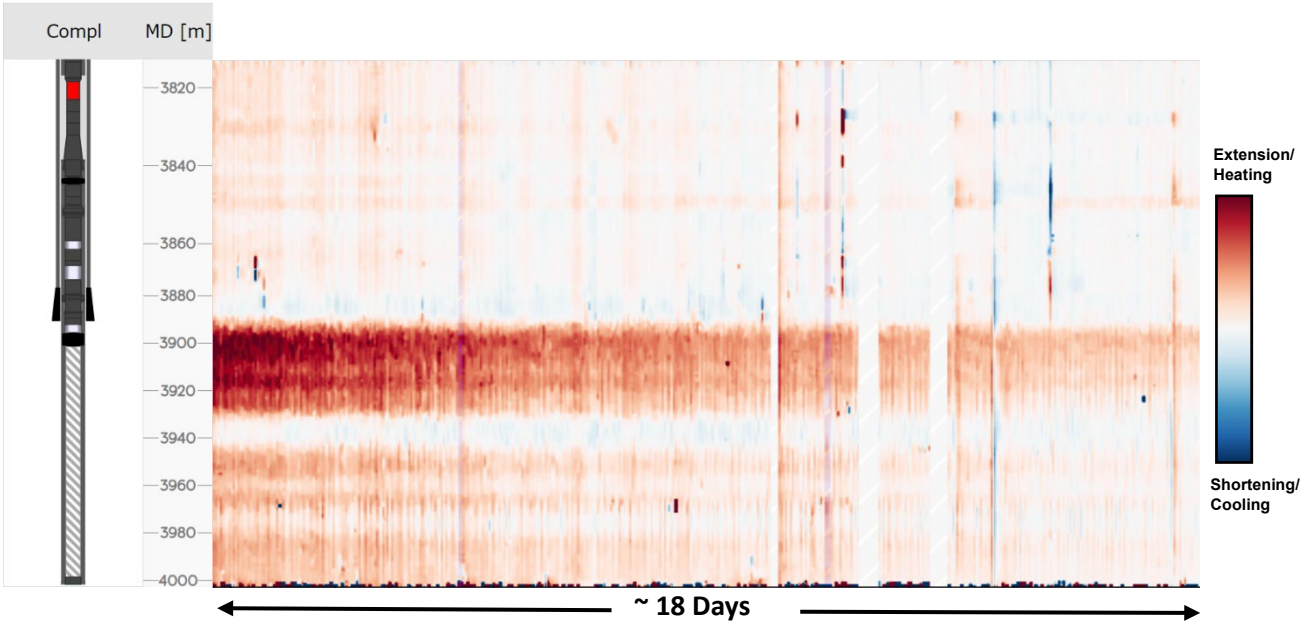

Figure 2: LF-DAS data from an injection well which has not started injection (measuring the change in phase). Display shows a warm-back period of around three weeks, heating up to original temperatures after a loss of liquids during completion of the well. The horizontal axis corresponds to increasing time from left to right and the vertical axis represents the depth along the well (mRKB).

To make a direct comparison of the two datasets (output temperature in °$\boldsymbol{C}$), restructuring and conditioning of the data is carried out. The first step involves putting the datasets on a new grid in time, taking into account the different sampling parameters of each dataset. Next, the time derivative of the DTS data is taken. The output of the data is now having units of degrees per second (°$\boldsymbol{C/s}$) which corresponds to the time derivative of strain in LF-DAS data. This is expected theoretically because the optical phase is sensitive to temperature, as shown in Eq. 3. LF-DAS measures the rate of change of the phase, making us sensitive to the rate of temperature change.

As shown in **Fig. 3**, a median filter in time is applied to remove the effects of strain. In this example, effects related to strain display much higher amplitudes than the background temperature response of LF-DAS data and are likely due to strain on the tubing. Strain on the tubing exhibits wave speeds of 4500-5000 m/s (steel velocity), as opposed to strain on the fibre itself (~2000 m/s). Since the fibre is clamped to the tubing, it can experience strain on the tubing from various sources, including mechanical strain due to flow-induced friction and pistoning etc. (Haavik, 2022). An example of strain acting on the fibre can be due to temperature changes that induce axial strain on the fibre. If simple averaging of the data is applied by increasing the decimation factor when resampling, the dipole-like feature will remain and in some cases merge into larger dipoles linked to strain. The dipole character of the signal shows the effect of the tubing moving upwards, signifying movement in a limited depth range with the colour code red indicating downward movement with respect to the measured depth. Hence, to effectively remove the dipole-like features, filtering over time is required. This filter needs to be applied over a long period to effectively remove the tails of dipole strain features. The more laterally extensive

high amplitude signals are unwrapping errors which can be removed by applying a median filter along the depth axis. If any pressure or strain effects remain after filtering, thresholding of high-frequency events is performed to remove these. In any case, it is unlikely that all strain and pressure effects can be removed in their entirety, adding uncertainty to the subsequent analysis.

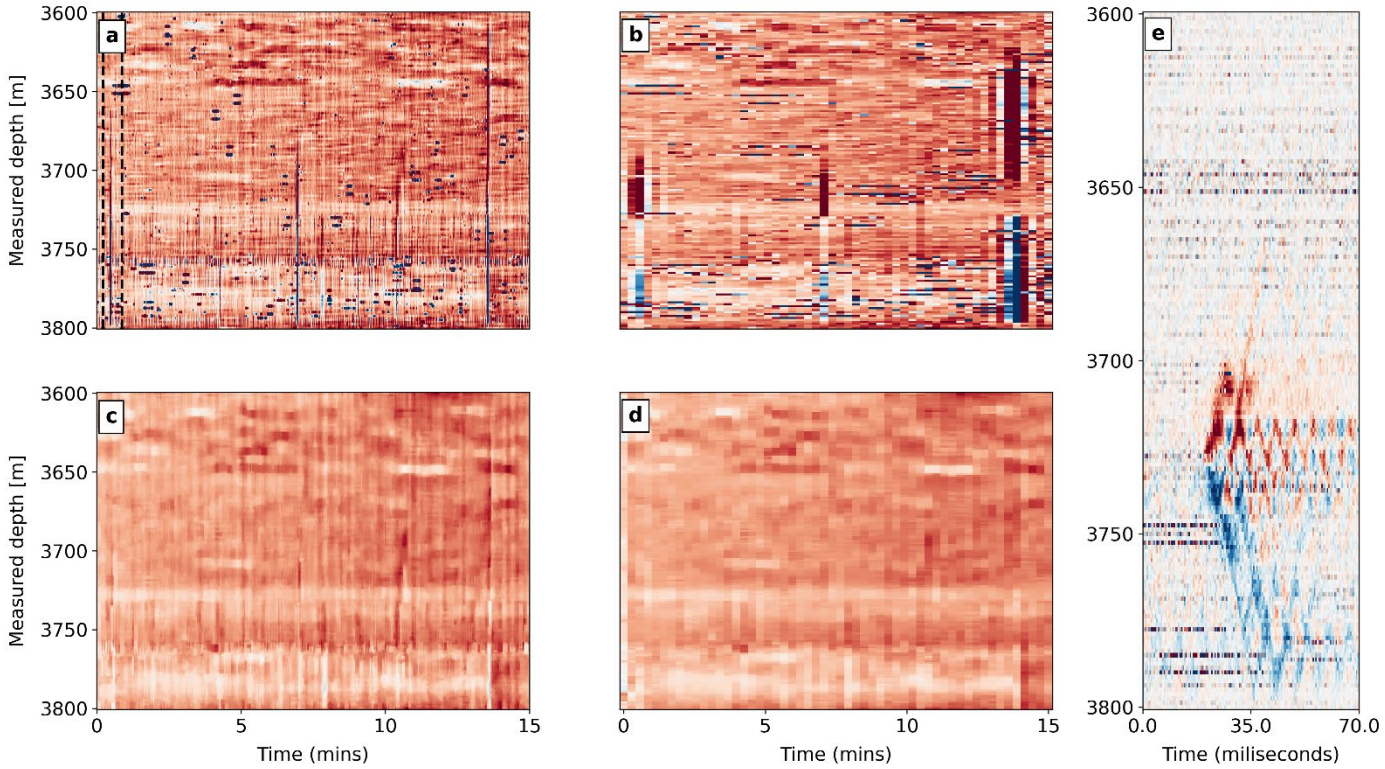

Figure 3: Filtering of strain/pressure effects in LF-DAS data measuring phase change. Colour-scale: red corresponds with extension/heating and blue represents shortening/cooling. (a) LF-DAS data showing strain and pressure effects overlaying background temperature. Numerous dipole-like features linked to strain effects visible on LFDAS data alongside other high amplitude events (unwrapping errors). These effects are much higher amplitude than those generated because of temperature variation (x10000 amplitude compared to the temperature gradient). Not likely that these high-amplitude events could create time strain associated with temperature and are likely due to strain and pressure effects. (b) resampled LF-DAS data with higher decimation factor, (c) median filtered data in time and space of 3(a), (d) median filtered data in time and space of 3(b), (e) dipole feature showing displacement that can't be averaged out, signified by red above and blue below (wave speed ~4500-5000 m/s, Nyquist frequency 1250 Hz) from data that closer resembles raw LF-DAS data (lower decimation factor), highlighted by the dashed vertical lines from 3(a).

The datasets are then aligned in depth by using depth calibration reference points in the well (e.g., clamp depths) and put onto the same grid in depth. This process is performed after denoising the LF-DAS data to avoid interpolation between high-frequency strain events. The DTS data is smoothed by convolving it with a suitable filter, followed by noise subtraction by taking the smoothed DTS data over a specific depth range away from the entire smoothed dataset. Smoothing is applied to the DTS data due to numerous vertical stripes correlated with depth linked to measurement noise.

A linear regression is applied to find a single scaling factor to multiply with LF-DAS data to make it equivalent to the time derivative of DTS data. The inputs for the regression are the filtered LF-DAS data and the smoothed time derivative of the DTS data, outputting a scaling factor for each depth (the integral of these inputs is additionally tested). The resultant scaling factor output has an inherent link to data quality. If the noise is larger than the signal, then the regression analysis becomes more uncertain. This is observed in the estimation of the scaling factor corresponding to each depth (**Fig. 4**). The depth range where the main heat-back effect is observed are marked by dashed lines (3902 – 3928m MD). This zone exhibits the clearest signal, hence, outputting the most accurate scaling factor for this dataset. Within this zone we observe a stable result ranging from 0.002 – 0-0032 $°C/rad$. The scaling factor values output in the depth range where we have little to no signal are discarded and not used in this analysis. The validity of using linear regression is justified by the cross-plots. We present the cross-plot for both temperature vs. phase and temperature rate vs. phase change, comparing the main warm-back period to an interval where only noise is observed. In the main warm-back period, we clearly observe a trend between temperature/temperature change and phase/phase change, whereas no such trend is apparent in the noise interval. The plotted linear trend has a gradient equivalent to the mean value from the regression analysis. As observed here, deviation from the main trend will increase the uncertainty in the results, and we believe that the noise from DTS data plays a significant role in this regard.

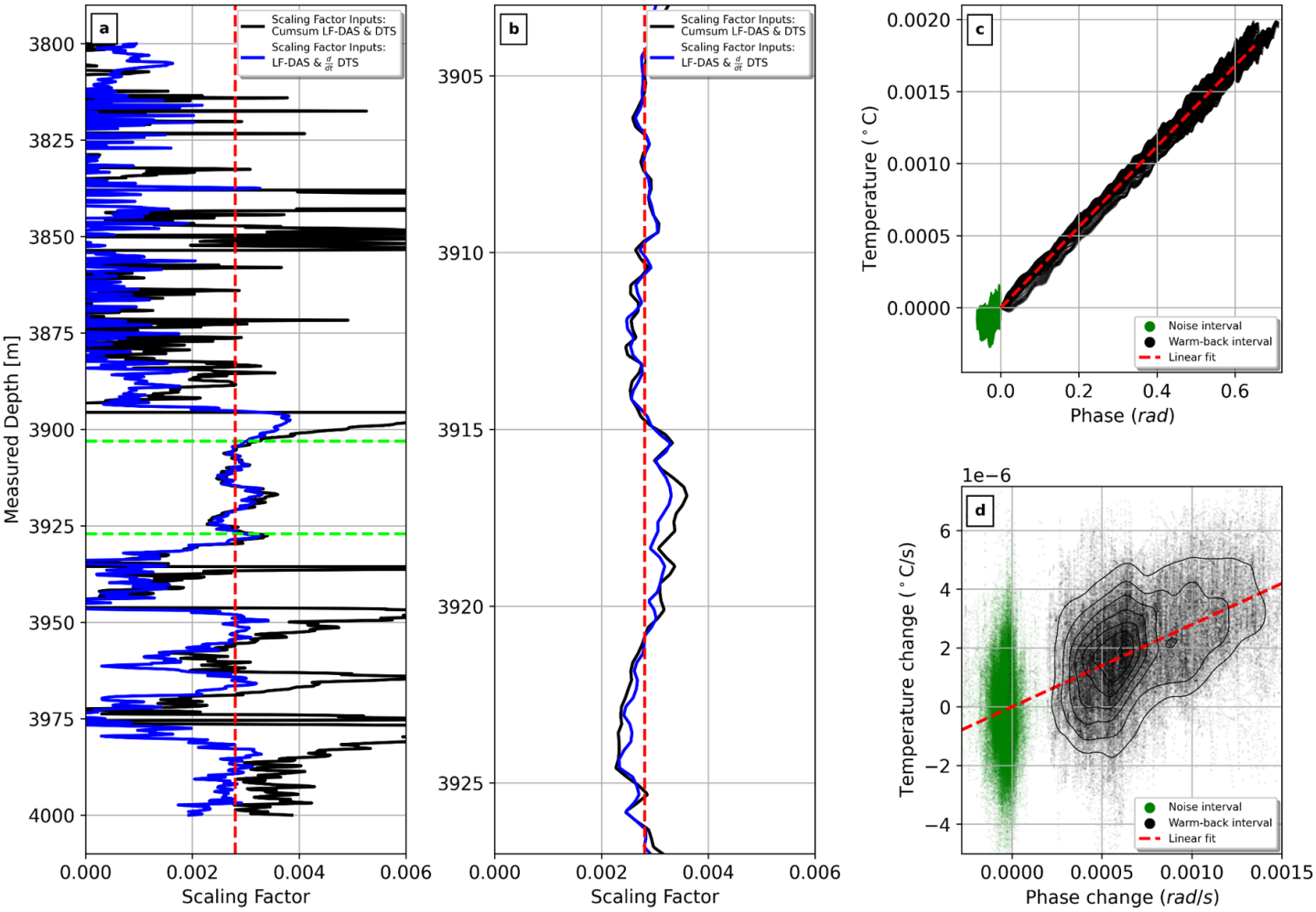

Figure 4: Linear regression – find scaling factor to apply to LF-DAS data. (a) calculated scaling factor corresponding to each depth. Dashed horizontal lime-green lines mark the zone where main warm-period is observed (3902 – 3928m MD). (b) depths corresponding to the main warm-back period are shown here with a scaling factor ranging between 0.002 - 0.0032. Dashed red vertical line corresponds to the mean value for the scaling factor within this interval. (c) cross-plot of phase vs. temperature showing the warm-back interval and a noisy interval. The best-fit line is chosen with a gradient equivalent to the mean of the regression analysis. (d) cross-plot of phase change vs. temperature change showing the warm-back interval and a noisy interval (best-fit line chosen as above with associated contour lines representing the probability density of the data).

The LF-DAS data can then be converted to temperature change by applying the appropriate scaling factor to the entire dataset. A scaling factor of 0.0028 $°C/rad$ is chosen (mean value from regression analysis) and applied to the LF-DAS data to directly compare with the time derivative of the DTS data (**Fig. 5**). The chosen scaling factor value is used for the remainder of the analysis. The output of both datasets is in degrees per second ($°C/s$), with a profile over time chosen where temperature changes are observed (3915m MD). The scaled LF-DAS data matches the time derivative of the DTS trend generally well, just with smaller amplitudes and generally less noise due to prior pre-processing steps and inherent measurement noise associated with DTS systems. The absolute temperature recording from the DTS data is additionally shown for the same trace alongside the integral of the LF-DAS data. This demonstrates that although the change in temperature shows good correspondence between the two datasets, absolute temperature recordings from LF-DAS data require reference temperatures to match the DTS data.

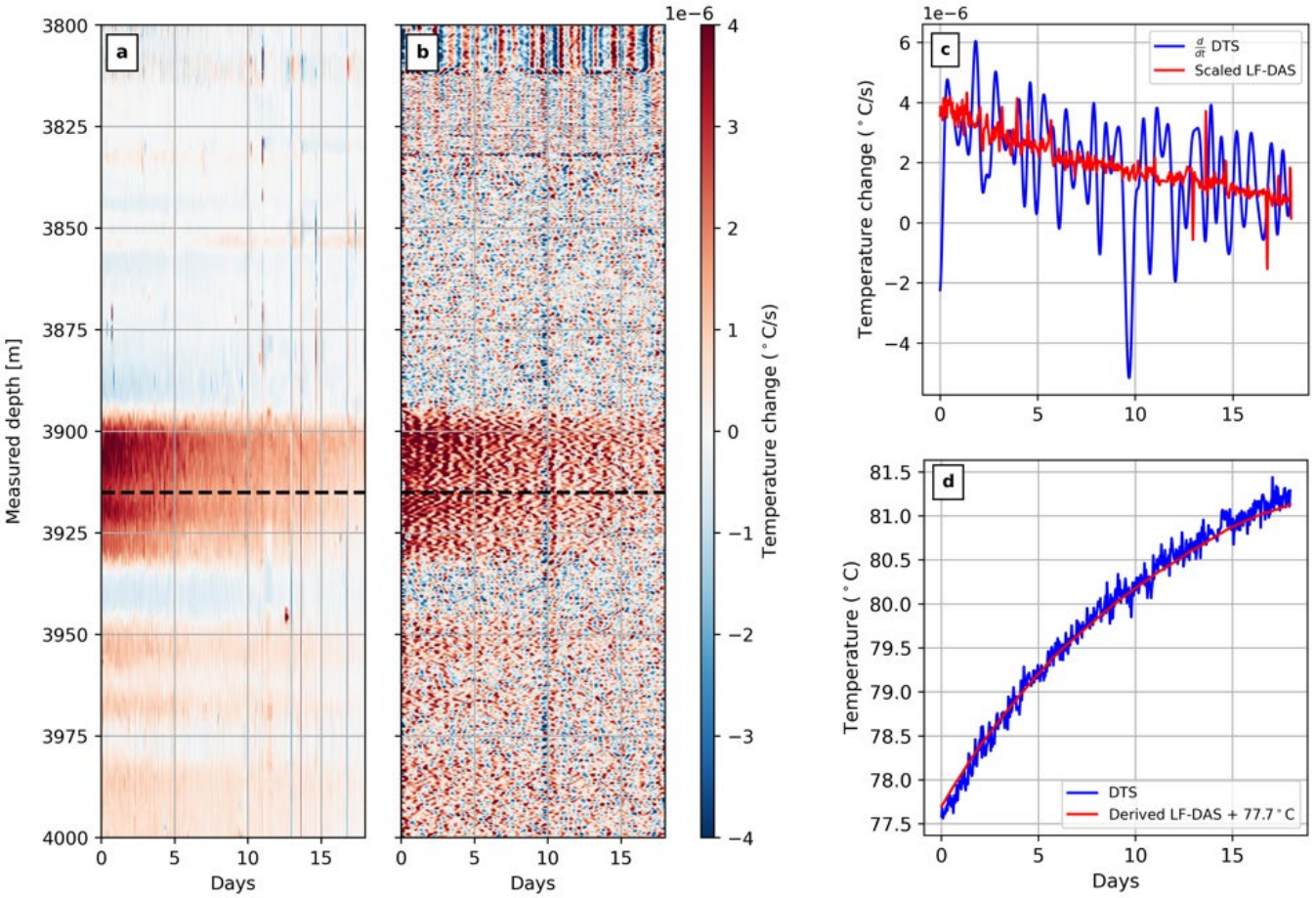

Figure 5: (a) Filtered LF-DAS data multiplied by chosen scaling factor (0.0028 $°C/rad$), (b) $\frac{d}{dt}$DTS - the time derivative of the smoothed DTS data outputting $°C/s$. (c) a profile over time corresponding to the dashed horizontal line (3915m MD) in a period where we observe temperature variation (blue – $\frac{d}{dt}$DTS , red – Scaled LF-DAS). (d) equivalent profile over the entire time range but taking the integral from LF-DAS + 77.7$°C$ alongside the DTS temperature traces to output absolute temperature in $°C$.

The integral of both datasets (scaled LF-DAS and the time derivative of the DTS) results in temperature values in $°C$. To directly compare the DTS data (absolute temperature values) with the LF-DAS data, a reference temperature must be added to the LF-DAS data. This reference point can either be from the first timestamp of the DTS data or from a linear temperature trend between the heel and toe temperature gauges in the reservoir zone. The integral of the scaled LF-DAS data with the addition of the reference DTS temperature is directly comparable with the DTS temperature traces **(Fig. 6)**. In particular, the main warm-back period between 3900-3930m shows a strong correlation. However, weaker signals associated with other warm-back effects at greater depths in the well show a poorer resolution in the integral of the scaled LF-DAS data when compared with the DTS data. This may be due to strain/pressure effects which have not been removed in the described processing steps, altering the temperature response of the LF-DAS recording. Hence, filtering of the strain/pressure effects is seen as the key limitation in the methodology. A summary of the processing steps is illustrated in **Fig. 7**.

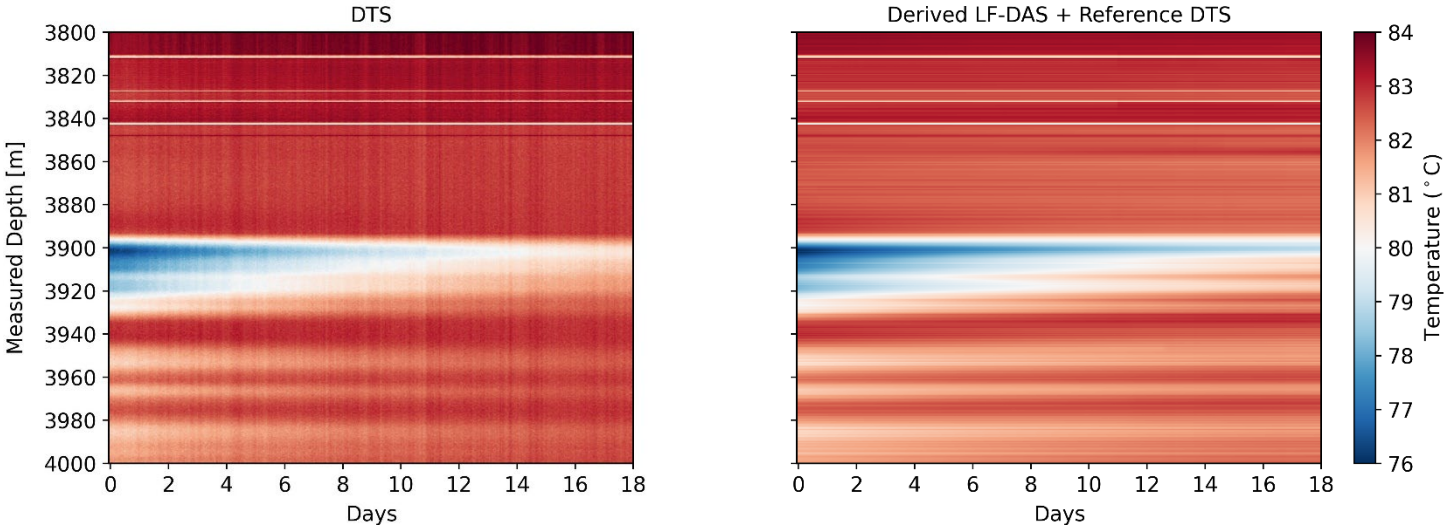

Figure 6: Left: observed temperature change for DTS data. Right: the integral over time of the LF-DAS data multiplied by the chosen scaling factor (0.0028) with the initial temperature profile of the DTS data added as a starting reference point.

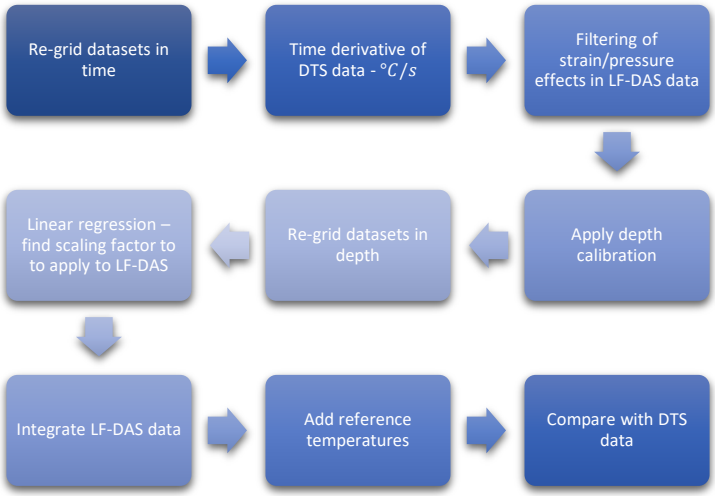

Figure 7: Flowchart of the processing workflow undertaken to acquire the temperature response of LF-DAS data to directly compare to DTS temperature data ($°C$).

Temperature Profiling

Monitoring for flow profiling of in-well measurements can provide valuable information to make production-based decisions real-time, potentially avoiding costly choices such as an intervention job. Additionally, monitoring of temperature changes in the overburden or reservoir can be valuable in the life cycle of a maturing well. In the past, temperature logs have been used to quantitively estimate flow rates at different positions in the wellbore (Curtis and Witterholt 1973). With the emergence of fibre as a sensing tool for in-well measurements, DTS systems have additionally been implemented to determine flow profiles (Ouyang and Belanger 2006). Although these prescribed systems output a valid result, the limitations associated with standard approaches make it desirable to utilise LF-DAS data as a verification tool to monitor geothermal gradients in wells. This is particularly applicable for monitoring variations in temperature trends in the overburden.

Temperature changes observed in a well can be attributed to a multitude of factors with varying temporal distributions. For example, heat transfer effects due to variations in the properties of the formation (e.g., more permeable zones), changes in fluid levels in the well, shifts in the deviation of the wellbore, presence of different phases in the well (gaseous phase heating faster), displacement of the fluid column due to injection etc. Prior to this, we have shown that LF-DAS data contains high-quality temperature information and is well suited for monitoring temperature variations. However, the main drawback is that it cannot yield absolute temperature values. Here, we show that given that there is an initial flow in the wellbore – we can estimate the absolute temperature profiles with the aid of gauge data.

In the upcoming analysis we aim to map out the temperature profile that purely accounts for the displacement of the fluid column. This implies that the result will only be valid at the initial point of displacement, which occurs in the order of minutes, and not at later times where other heat transfer effects must be considered. This is done by assuming that heat transfer through the production tubing is much faster than the heat transfer through the subsequent annuli and formation. However, since the measurement is acquired on the outer side of the tubing, we rely on heat transfer through the tubing. This suggests that it takes time before the temperature is measured at the fibre and that heat transfer effects are slower than the change in temperature due to movement of the

fluid column, i.e., heat transfer is ignored since it is a slow process. In addition, we assume that the temperature in the tubing is equal to the initial temperature with some form of displacement. With these assumptions in mind, the initial temperature profile $\boldsymbol{T_i}$ due to displacement of the fluid column can be expressed as (Appendix A – derivative over depth with a scaling factor is approximately equivalent to derivative over time):

$$\boldsymbol{T_i(z) = a \times \left(-\frac{1}{v}\int_{z_0}^{z} \frac{\partial T(z')}{\partial t}\, dz'\right) + c} \quad (5)$$

where $\frac{\partial T(z',t)}{\partial t}$ is the time derivative of the temperature response proportional to the LF-DAS data, $\boldsymbol{v}$ corresponds to the apparent displacement velocity, while $\boldsymbol{a}$ and $\boldsymbol{c}$ are a scaling factor and constant, respectively, that depend on the background temperature response. The integral over depth of the data is subsequently shifted in accordance with the displacement of the fluid column. This displacement is defined based on the slope observed in the data. The scaling factor and constant parameters are linked with the reference temperatures from the wellhead and downhole temperature gauge. They are found by applying a simple inversion to find the scaling factor and constant to apply to the LF-DAS data to output the DTS temperature values. In essence, the reference temperatures around the top and bottom of the well aid in matching the corresponding LF-DAS and DTS temperature trends. Finally, the median of the resultant scaled and shifted LF-DAS data where displacement is observed is taken.

The resultant temperature profile from LF-DAS can then be compared with the initial DTS temperature profile. In theory, if the data is cleaned from strain and pressure effects and corresponds to the pure temperature response, then only a single gauge is required to map out the absolute temperature profile from LF-DAS data. This is in correspondence with **Fig. 6**, where we utilise a single reference point (DTS) to achieve this. However, if two gauges are present, as is the case in many offshore wells, then the scaling applied linked to displacement is not required as we essentially just fit two points in the depth integral.

To determine the practicality of applying LF-DAS as a tool for temperature profiling, a dataset is chosen which aims to avoid as many unwanted strain and pressure effects from the fibre as possible. The first example is from an injector well where we observe a change in the downhole choke pressure due to injection, inducing a displacement in the fluid column, with an apparent velocity of 0.05 m/s. Despite choosing a calm period in the well, various strain effects are observed. These effects add to the uncertainty in any upcoming temperature analysis and are mostly removed using the filtering approaches described above. The integral over depth of the LF-DAS data is taken and only remains valid in the initial period where displacement is occurring without other heat transfer effects. After fitting the integral to top- and downhole temperatures, it is observed that the estimated temperature profile from LF-DAS matches the DTS initial profile very well with strong correspondence at all depths **(Fig. 8)**.

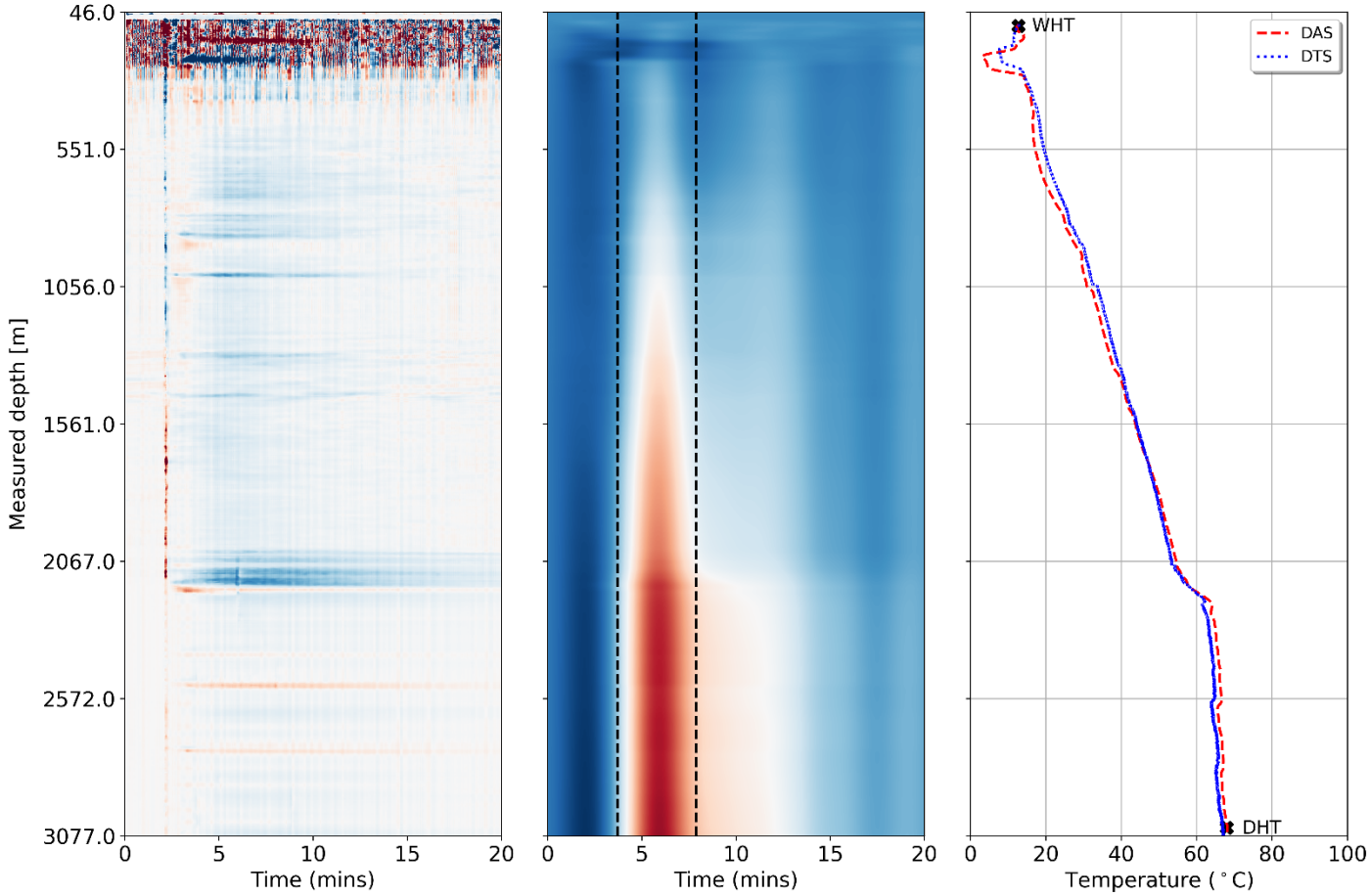

Figure 8: Temperature profiling of injector well using LF-DAS data. Left: median and frequency filtered LF-DAS data (phase change). Centre: integral over depth of LF-DAS data (phase). Right: comparison of the temperature profile from LF-DAS and the initial DTS temperature profile. The LF-DAS temperature profile is taken over the median of the time range where the initial displacement occurs marked with dashed vertical lines. Wellhead (WHT) and downhole gauge data (DHT) are used as reference temperature measurements to scale the LF-DAS profile (marked with black cross).

The same approach is shown for a producing well where the well has been shut in for a period prior to the choke being opened. Similarly, the output temperature profiles match relatively well (**Fig. 9**), particularly capturing subtle temperature changes observed in the DTS profile. The observed variation in temperature likely corresponds to a combination of factors, including changes in the general geothermal gradient with depth, fluctuations associated with changes in the geological formation and variations linked to the movement of fluids in the well.

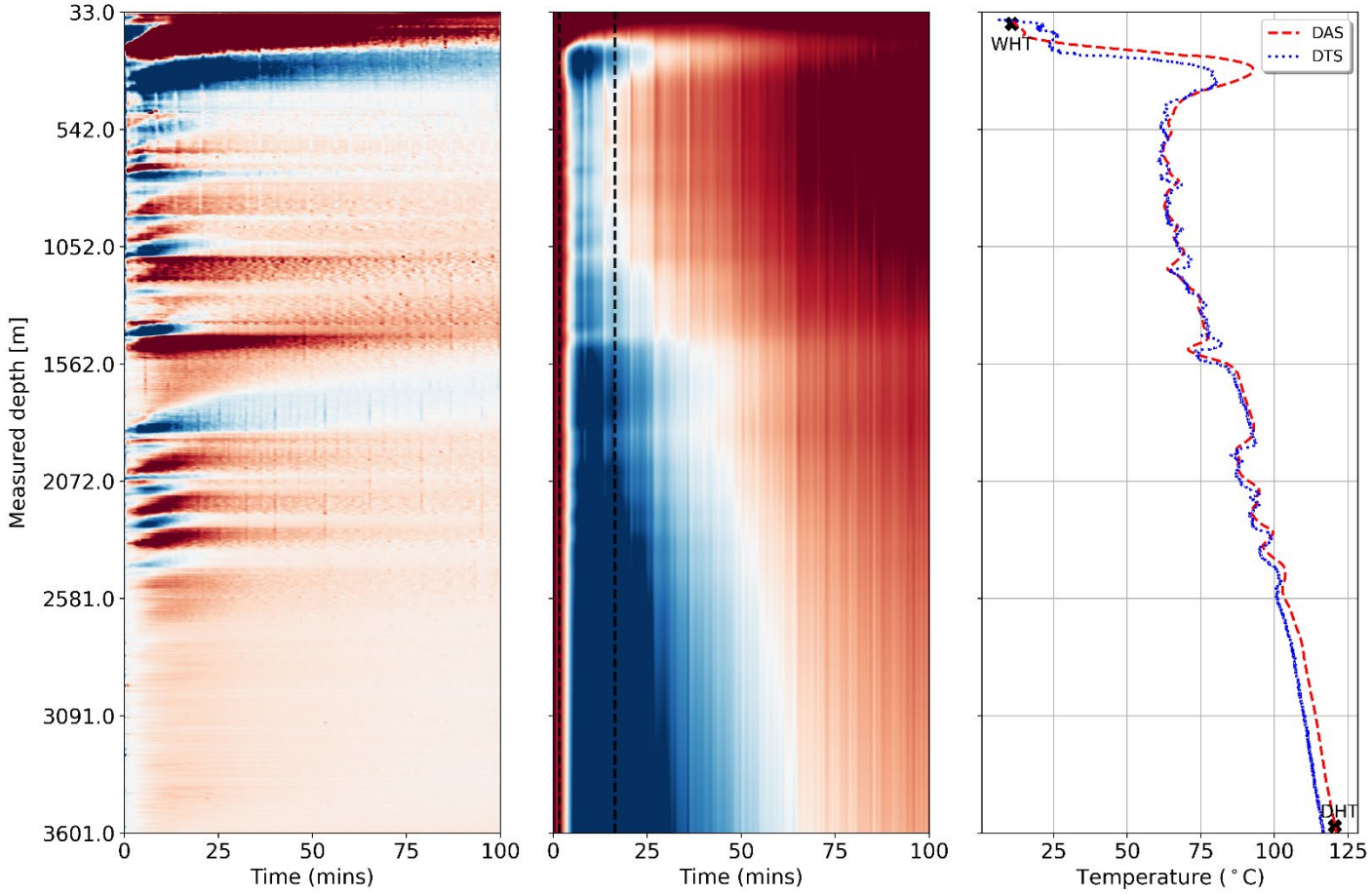

Figure 9: Temperature profiling of production well using LF-DAS data. Left: median and frequency filtered LF-DAS data (phase change). Centre: integral over depth of LF-DAS data (phase). Right: comparison of the temperature profile from LF-DAS and the initial DTS temperature profile. The LF-DAS profile is taken over the median of the time range where the initial displacement occurs marked with dashed vertical lines. Wellhead (WHT) and downhole gauge data (DHT) are used as reference temperature measurements to scale the LF-DAS profile (marked with black cross).

Although the above examples show a good proof of concept, it is important to highlight other cases which show potential limitations in the method. The next example we present is from another injection well. In this case, the glass plug in the reservoir zone is open, meaning the well is not sealed off from the reservoir. Cold water is injected from the top, and then the choke is slowly opened, thereby increasing the pressure. This pressure increase allows fluids to flow from top to bottom, causing the fluid column to shift downward and eventually end up in the reservoir **(Fig. 10)**. The displayed signal indicates fluids moving downward with an apparent velocity ranging from 0.1 - 0.2 m/s. The output temperature profile trends generally match well, however, the shallow portion of the datasets displaying a high amplitude blue/red event (43 – 500m MD) appears to skew the resultant LF-DAS profile. The shallow

interval used in this analysis signifies a rapid change in temperature which is poorly accounted for. This can be explained by the presence of a gas bubble (different heat capacity to the remainder of the fluid column) which would lead to a rapid change in temperature with changing pressure. It can also be explained by the effect of pistoning due to friction (Haavik, 2022) leading to strain effects which cannot be filtered out. Either of these effects cannot be accounted for in this analysis with the prescribed methodology. A further possible constraint in this approach is the requirement for the DTS data to be calibrated to fit with the wellhead and downhole gauge temperature measurements. If this condition is not met, the resulting temperature measurements at the shallowest and deepest points will not match, resulting in a constant drift between the two profiles.

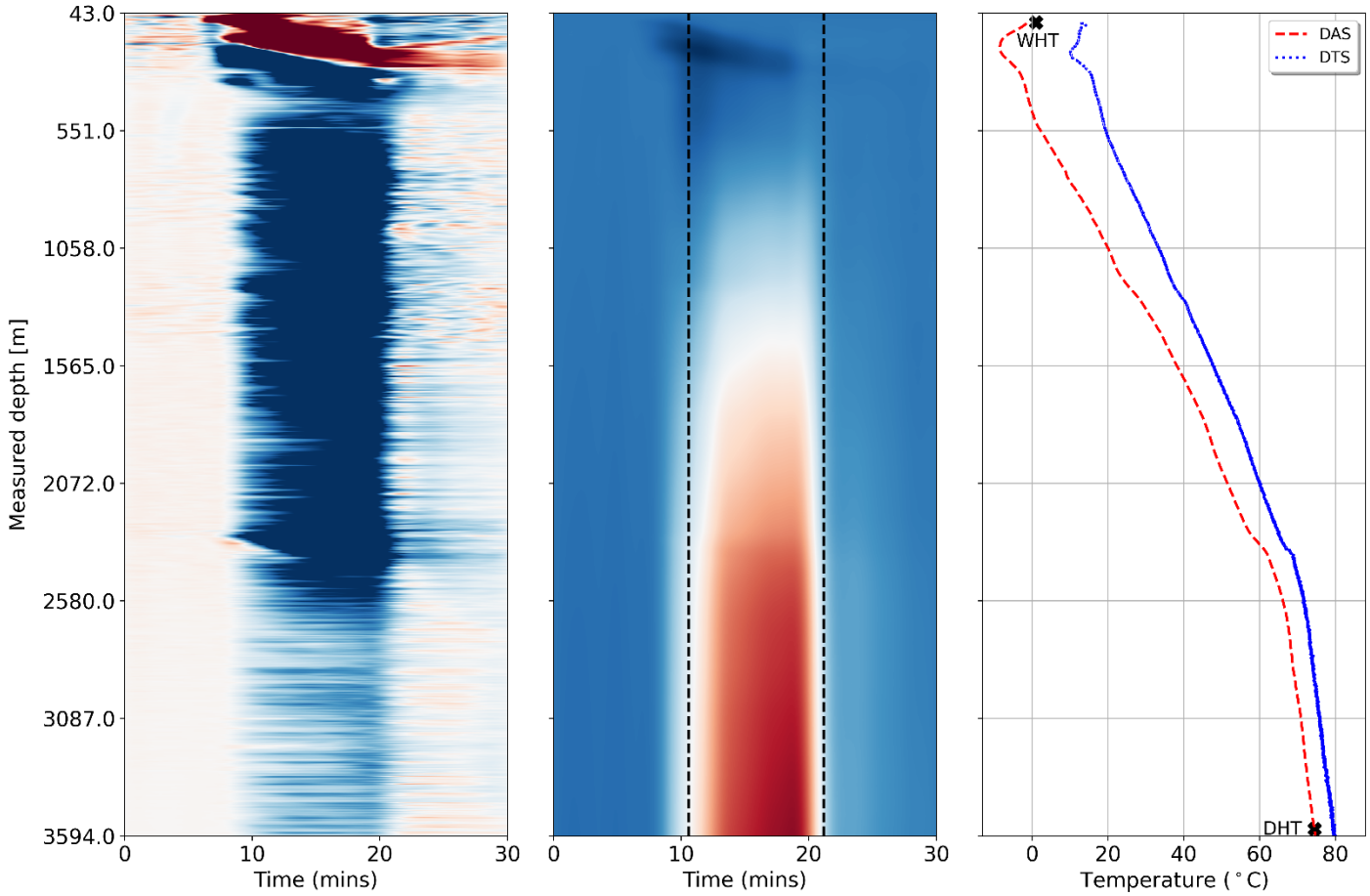

Figure 10: Temperature profiling of injector well using LF-DAS data. Left: median and frequency filtered LF-DAS data (phase change). Centre: integral over depth of LF-DAS data (phase). Right: comparison of the temperature profile from LF-DAS and the initial DTS temperature profile. The LF-DAS profile is taken over the median of the time range where the initial displacement occurs marked with dashed vertical lines. Wellhead (WHT) and downhole gauge data (DHT) are used as reference temperature measurements to scale the LF-DAS profile (marked with black cross). Shallow zone between 43 – 500m MD shows potential limitations in the method.

Ultimately, temperature profiling using LF-DAS would be most valuable where DTS data is not available, i.e., where we don't have any ground truth temperature recordings. Having demonstrated the robustness of the method through testing on various producing and injecting wells (**Fig. 8, 9**), the result is then examined on subsea wells. The final example is shown below from a subsea producing well **(Fig. 11)**. This case shows the fluid column being displaced after starting up the well. To clarify the accuracy of the result, a DTS

profile from another producing well from the same field, which has not started producing yet, is compared with the resultant LF-DAS profile. This also fits well with the derived LF-DAS profile, observing a shift in the gradient when entering a different geological formation (~1700m MD). Small deviations in the LF-DAS profile from the DTS profile are expected since the well will encounter the same geological formations, but at different depths. The large increase in temperatures observed in the DTS profile in the shallower zone is caused by heat up effects due to proximity of neighboring wells as they approach a manifold closer to surface. Hence, the profile at this depth interval is ignored.

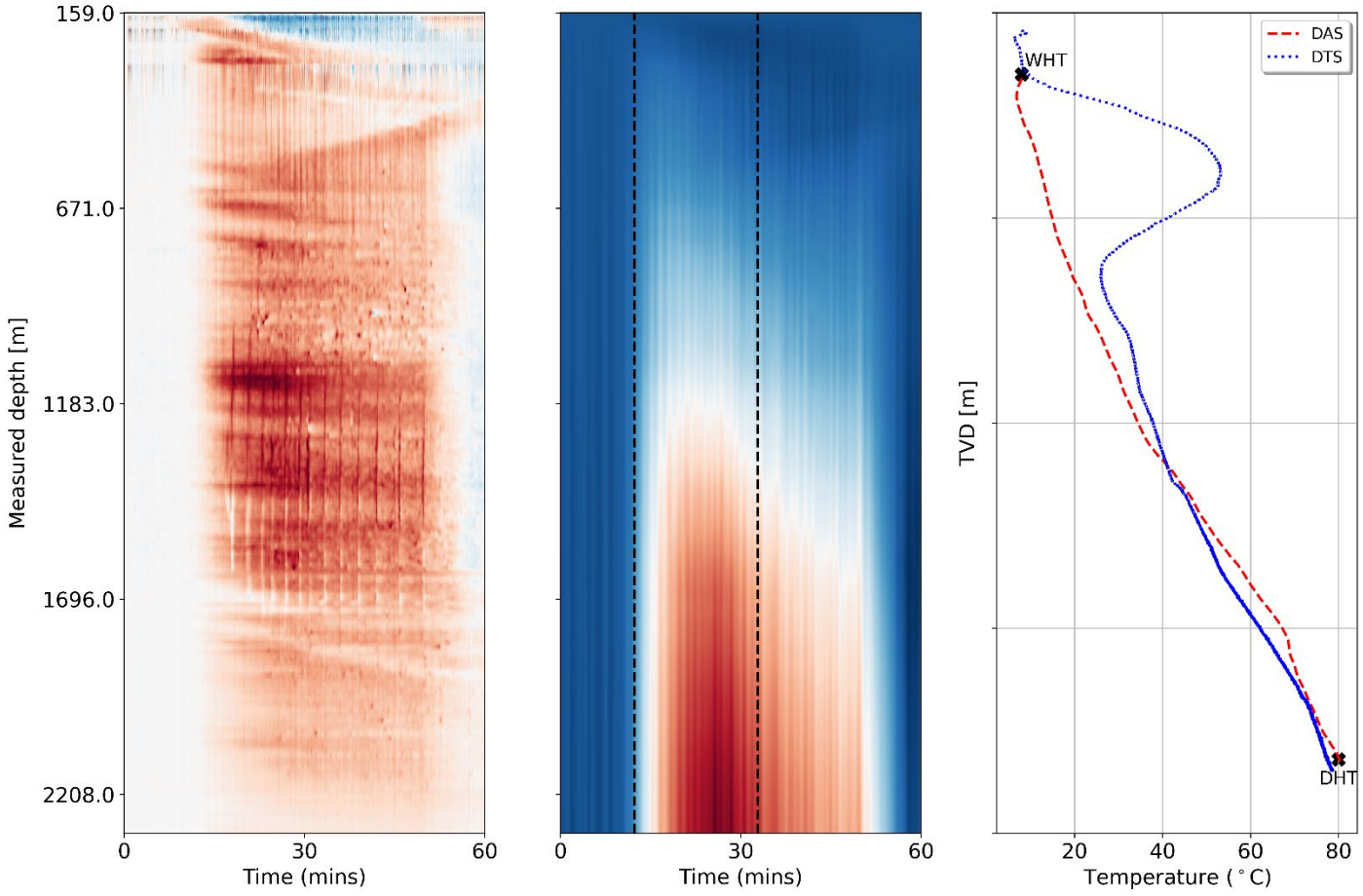

Figure 11: Temperature profiling of subsea producing well prior to start-up of production. Left: median and frequency filtered LF-DAS data (phase change). Centre: integral over depth of LF-DAS data (phase). Right: comparison of the temperature profile from LF-DAS and a DTS profile from a virgin well prior to production plotted in true vertical depth (TVD). The LF-DAS profile is taken over the median of the time range where the initial displacement occurs marked with dashed vertical lines. Wellhead (WHT) and downhole gauge data (DHT) are used as reference temperature measurements to scale the LF-DAS profile (marked with black cross).

Discussion

The LF-DAS data presented in this paper are found to be directly linked with the temperature gradient observed in DTS data (**Fig. 5**). The output strain rate measured by DAS is proportional to the time derivative of the temperature response obtained from DTS. Besides the signal related to the temperature response from LF-DAS, pressure and strain related events are usually present or coupled with the signal (**Fig. 3**). These effects are often easily visible when trying to pick out the so-called 'quiet' periods to track temperature

changes and normally provide useful information toward well monitoring. For example, observed pressure changes can be used to track leaks and other well integrity applications. Hence, although this study is primarily interested in the temperature response of LF-DAS data, some undesirable features linked to pressure and strain effects will remain in the final output result, adding to the uncertainty. Alongside monitoring temperature variation in wells, LF-DAS can also be applied to other useful examples where the fibre is clamped in place, for example, monitoring the temperature change along a pipeline.

Temperature profiling as described in this paper is derived using LF-DAS and reference temperature measurements. It is noted that some of the examples displayed that demonstrate temperature profiling are chosen opportunistically to avoid rapid changes in temperature associated with other heat transfer effects (**Fig. 8**). An example of operational procedures that work well for this approach would be opening the choke slowly thereby minimising the effect of flow induced strain or rapid pressure pulses in the LF-DAS data. Although the data is largely showing the effect of temperature, some pressure and strain related features remain which adds to the uncertainty in the final output result. In practice, if the choke is opened faster than the examples observed in this paper, it may increase the uncertainty in the result. However, the temperature profiles can still be used as they consistently capture the general temperature gradient effectively. We recommend using this method when the displacement velocity does not exceed 0.15 m/s**.**

It is important to consider another aspect in this method, which is that there is a fundamental difference in how the datasets are calibrated. LF-DAS data, as shown in this study are calibrated to the gauge measurements just prior to the well operation taking place as opposed to DTS which is calibrated to a bottom-hole temperature prior to deployment. This implies that the downhole temperature measurement derived from the LF-DAS profile, which is calibrated to the gauge, may, in fact, be more reliable than the DTS downhole measurement which we consider as our ground truth.

Theoretically, the result is only valid for the initial displacement and thus cannot be used for temperature profiling when other heat transfer effects are taking place (**Fig. 10**). The incorporation of additional heat transfer effects, such as estimating the thermal diffusivity of the fluid content at various depths in the well was found to increase the complexity of the model without enhancing the final output temperature profile result. Therefore, the simpler model has been employed in this study. Another potential limitation in the approach is the reliance on reference temperature points to output the final profile. However, most offshore wells will constitute at least two reference temperature points which can be utilised to better fit the profile. Therefore, despite these shortcomings, LF-DAS can be seen as a valuable tool to estimate temperature profiles, particularly in subsea wells with long lead-in lengths where DTS data is rarely available without the use of additional technology to enhance the signal.

Conclusions

We have shown that LF-DAS can be used to monitor temperature changes over long time periods (several weeks) with high accuracy. The LF-DAS output, strain rate, is linearly proportional to the time derivative of the temperature response observed in DTS data with a scaling factor applied. This conversion varies depending on the dataset analysed and can only be derived where we observe a clear signal associated with temperature. In addition, we show that incorporating DTS reference temperature measurements or temperature gauge data allows for the comparison of absolute temperature variation. The validity in extracting the temperature response of LF-DAS data is dependent on choosing a period which avoids any undesirable strain and pressure effects, i.e., a ‘quiet’ period in the well. Hence, appropriate filtering of the data is regarded as crucial in acquiring the temperature response from LF-DAS data.

A further application for using LF-DAS toward temperature profiling was then explored. Temperature profiles derived from LF-DAS data linked to the initial displacement of the fluid column are shown to be highly comparable to DTS initial temperature

profiles over the same interval. Implementation of LF-DAS toward temperature profiling is particularly relevant for subsea wells with long lead-in lengths as shown in the examples for both injecting and producing wells. This is due to the difficulty in deploying DTS measurements in longer wells without the use of costly technology such as optical circulators. The result is inherently dependent on utilising reference point measurements from the wellhead and downhole gauge; however, these measurements are present in nearly all wells. The accuracy of the result is reliant on avoiding other heat transfer effects later in time.

The data analysis undertaken shows that LF-DAS can be used as a temperature sensor for a variety of regular well-operations, for example, when monitoring warm-back effects linked to production over several weeks or more short-term temperature changes linked to unloading in the wellbore to induce flow. Ultimately, the flexibility of LF-DAS as a multipurpose sensor measuring strain, pressure and temperature effects will drive further applications to be developed in this space.

Acknowledgments

This work was supported by the SFI Centre for Geophysical Forecasting (grant 309960). The authors would like to thank the fibre-optics team at Equinor for the discussions related to the study. Thanks also go out to the partners in the Johan Sverdrup field, Equinor ASA, Aker BP ASA, Petoro AS and TotalEnergies E&P Norway AS and to the partners in the Martin Linge field, Equinor ASA, Petoro AS and Sval Energi AS for allowing us to use and publish the data. The views and opinions expressed in this paper are of those of the authors and are not necessarily shared by the license partners.

References

Bakku, S. K., Sudhish, K., Peter Wills, P., & Michael Fehler, M. 2014. Monitoring hydraulic fracturing using distributed acoustic sensing in a treatment well. In *2014 SEG Annual Meeting*.

Bakku, S. K. 2015. *Fracture characterization from seismic measurements in a borehole* (Doctoral dissertation, Massachusetts Institute of Technology).

Bouffaut, L., Taweesintananon, K., Kriesell, H. J., Rørstadbotnen, R. A., Potter, J. R., Landrø, M., Johanesen, S. E., Brenne, J. K., Haukanes, A., Schjelderup, O., & Storvik, F. 2022. Eavesdropping at the speed of light: Distributed acoustic sensing of baleen whales in the Arctic. *Frontiers in Marine Science,* 994.

Budiansky, B., Drucker, D. C., Kino, G. S., & Rice, J. R. 1979. Pressure sensitivity of a clad optical fiber. *Applied optics*, *18*(24), 4085-4088.

Cannon, R., & Aminzadeh, F. 2013. Distributed acoustic sensing: State of the art. In *SPE Digital Energy Conference*.

Curtis, M. R., & Witterholt, E. J. 1973. Use of the temperature log for determining flow rates in producing wells. In *Fall Meeting of the Society of Petroleum Engineers of AIME*.

Fang, Z., Chin, K., Qu, R., & Cai, H. 2012. *Fundamentals of optical fiber sensors* (Vol. 226). John Wiley & Sons.

Farahani, M. A., & Gogolla, T. 1999. Spontaneous Raman scattering in optical fibers with modulated probe light for distributed temperature Raman remote sensing. *Journal of Lightwave Technology*, *17*(8), 1379.

Fidaner, O. 2017. Downhole multiphase flow monitoring using fiber optics. In *SPE Annual Technical Conference and Exhibition*.

Foo, D., Krislock, J., Meador, T., & Cheng, T. 2014. Horizontal Well Injection Profiling Using Distributed Temperature

Sensing. In *SPE/CSUR Unconventional Resources Conference–Canada*.

Gao, H., Jiang, Y., Cui, Y., Zhang, L., Jia, J., & Jiang, L. 2018. Investigation on the thermo-optic coefficient of silica fiber within a wide temperature range. *Journal of Lightwave Technology*, *36*(24), 5881-5886.

Haavik, K. E. 2022. On the Use of Low-Frequency Distributed Acoustic Sensing Data for In-Well Monitoring and Well Integrity: Qualitative Interpretation. *SPE Journal*, 1-16.

Hartog, A. H. 2017. *An introduction to distributed optical fibre sensors*. CRC press.

Horst, J. V., Al-Bulushi, N., Deitrick, G., Mustafina, D., Hemink, G., Groen, L., Potters, H., Mjeni, R., Awan, K., Rajhi, S., & Bakker, G. 2015. Latest developments using fiber optic based well surveillance such as distributed acoustic sensing (DAS) for downhole production and injection profiling. In *SPE Kuwait Oil and Gas Show and Conference.*

Izgec, B., Kabir, S., & Hasan, A. R. 2006. Transient fluid and heat flow modeling in coupled wellbore/reservoir systems. In *SPE Annual Technical Conference and Exhibition*.

Jin, G., Friehauf, K., Roy, B., Constantine, J. J., Swan, H. W., Krueger, K. R., & Raterman, K. T. 2019. Fiber optic sensing-based production logging methods for low-rate oil producers. In *SPE/AAPG/SEG Unconventional Resources Technology Conference.*

Johannessen, K., Drakeley, B., & Farhadiroushan, M. 2012. Distributed acoustic sensing-a new way of listening to your well/reservoir. In *SPE Intelligent Energy International*.

Johnson, D. O., Sierra, J. R., Kaura, J. D., & Gualtieri, D. 2006. Successful flow profiling of gas wells using distributed temperature sensing data. In *SPE Annual Technical Conference and Exhibition*.

Kabir, C. S., Izgec, B., Hasan, A. R., Wang, X., & Lee, J. 2008. Real-time estimation of total flow rate and flow profiling in dts-instrumented wells. In *International Petroleum Technology Conference*.

Karrenbach, M., Ridge, A., Cole, S., Boone, K., Kahn, D., Rich, J., Silver, K., & Langton, D. 2017. DAS microseismic monitoring and integration with strain measurements in hydraulic fracture profiling. In *Unconventional Resources Technology Conference, Austin, Texas, 24-26 July 2017* (pp. 1316-1330). Society of Exploration Geophysicists, American Association of Petroleum Geologists, Society of Petroleum Engineers.

Karrenbach, M., Cole, S., Ridge, A., Boone, K., Kahn, D., Rich, J., Silver, K., & Langton, D. (2019). Fiber-optic distributed acoustic sensing of microseismicity, strain and temperature during hydraulic fracturing. *Geophysics*, *84*(1), D11-D23.

Koelman, J. M., Lopez, J. L., & Potters, J. H. 2012. Optical fibers: the neurons for future intelligent wells. In *SPE Intelligent Energy International*.

Lauber, T., & Lees, G. 2020. Enhanced temperature measurement performance: Fusing DTS and DAS results. *IEEE Sensors Journal*, *21*(6), 7948-7953.

Leggett, S., Sakaida, S., Zhu, D., Hill, A. D., & Kerr, E. (2023). Interpretation of Fracture Initiation Points by In-Well Low-Frequency Distributed Acoustic Sensing in Horizontal Wells. *SPE Journal*, 1-10.

Leone, A., Galli, G., Drago, A., & Brown, G. 2015. Characterizing reservoir thermofacies by using distributed temperature sensing measurements. In *SPE Annual Technical Conference and Exhibition*.

Lindsey, N. J., Rademacher, H., & Ajo-Franklin, J. B. 2020. On the broadband instrument response of fiber-optic DAS arrays. *Journal of Geophysical Research: Solid Earth*, *125*(2).

Malanya, G., Butula, K., Burdin, K., Khaziev, M., Kuzmin, S., Kaeshkov, I., & Kremenetskiy, M. 2016. Successful Experience of

Estimating Injection Flow Profile in Horizontal Wells Completed with Multistage Fracs in Conventional Reservoirs Using CT Conveyed Distributed Temperature Sensing. In *SPE Russian Petroleum Technology Conference and Exhibition*.

Mao, Y., Zeidouni, M., & Duncan, I. 2017. Temperature analysis for early detection and rate estimation of CO2 wellbore leakage. *International Journal of Greenhouse Gas Control*, *67*, 20-30.

Mestayer, J., Cox, B., Wills, P., Kiyashchenko, D., Lopez, J., Costello, M., Bourne, S., Ugueto, G., Lupton, R., Solano, G., Hill, D., & Lewis, A. 2011. Field trials of distributed acoustic sensing for geophysical monitoring. In *SEG technical program expanded abstracts 2011* (pp. 4253-4257). Society of Exploration Geophysicists.

Ouyang, L. B., & Belanger, D. 2006. Flow profiling by Distributed Temperature Sensor (DTS) system—Expectation and reality. *SPE Production & Operations*, *21*(02), 269-281.

Raab, T., Reinsch, T., Aldaz Cifuentes, S. R., & Henninges, J. 2019. Real-time well-integrity monitoring using fiber-optic distributed acoustic sensing. *SPE Journal*, *24*(05), 1997-2009.

Roy, R., Agrawal, D. K., & McKinstry, H. A. 1989. Very low thermal expansion coefficient materials. *Annual Review of Materials Science*, *19*(1), 59-81.

Seabrook, B. C., Ellmauthaler, A., LeBlanc, M., Jaaskelainen, M., Maida, J. L., & Wilson, G. A. 2022. Comparison of Raman, Brillouin, and Rayleigh Distributed Temperature Measurements in High-Rate Wells. In *SPWLA 63rd Annual Logging Symposium*.

Schuberth, M. G., Bakka, H. S., Birnie, C. E., Dümmong, S., Haavik, K. E., Li, Q., Synnevåg, J. F., Saadallah, Y., Vinje, L.,& Constable, K. 2021. A real-time fiber optical system for wellbore monitoring: A Johan Sverdrup case study. In *SPE Offshore Europe Conference & Exhibition*.

Sharma, H., Al-Zain, A., Al-Salman, N., Al-Harbi, M., & Said, R. 2010. A Successful Application of Permanently Installed Distributed Temperature Sensing (DTS) for Optimization of Acid Treatment in Power Water Injector with Advanced Well Completion: Case Study. In *SPE Annual Technical Conference and Exhibition*.

Sherman, C., Mellors, R., Morris, J., & Ryerson, F. 2019. Geomechanical modeling of distributed fiber-optic sensor measurements. *Interpretation*, *7*(1), SA21-SA27.

Shiach, G., Nolan, A., McAvoy, S., McStay, D., Prel, C., & Smith, M. 2007. Advanced feed-through systems for in-well optical fibre sensing. In *Journal of Physics: Conference Series* (Vol. 76, No. 1, p. 012066). IOP Publishing.

Sidenko, E., Tertyshnikov, K., Lebedev, M., & Pevzner, R. 2022. Experimental study of temperature change effect on distributed acoustic sensing continuous measurements. *Geophysics*, *87*(3), D111-D122.

Smith, R. G. 1972. Optical power handling capacity of low loss optical fibers as determined by stimulated Raman and Brillouin scattering. *Applied optics*, *11*(11), 2489-2494.

Soroush, M., Mohammadtabar, M., Roostaei, M., Hosseini, S. A., Mahmoudi, M., Keough, D., Cheng, L., Moez, K., & Fattahpour, V. 2021. An industry overview of downhole monitoring using distributed temperature sensing: Fundamentals and two decades deployment in oil and gas industries. In *SPE Western Regional Meeting*.

Wang, X., & Bussear, T. R. 2011. Real time horizontal well monitoring using distributed temperature sensing (dts) technology. In *OTC Brasil*.

Webster, P., Wall, J., Perkins, C., & Molenaar, M. 2013. Micro-seismic detection using distributed acoustic sensing. In *SEG Technical Program Expanded Abstracts 2013* (pp. 2459-2463). Society of Exploration Geophysicists.

Wilson, G. A., Seabrook, B. C., Moe, S., Suh, K., Jaaskelainen, M., Ellmauthaler, A., Bush, J., & Dupree, J. 2022. Distributed

acoustic sensing of long subsea tie-backs. In *Second International Meeting for Applied Geoscience & Energy* (pp. 647-651). Society of Exploration Geophysicists and American Association of Petroleum Geologists.

Xiao, J. J., Farhadiroushan, M., Clarke, A., Abdalmohsen, R. A., Alyan, E., Parker, T. R., Shawash J., & Milne, H. C. 2014. Intelligent distributed acoustic sensing for in-well monitoring. In *SPE Saudi Arabia Section Technical Symposium and Exhibition*.

Appendix A – Derivation for initial temperature profile due to displacement

The initial temperature profile due to displacement of a fluid column can be found by making the following assumptions. First, we assume that the temperature in the tubing is equal to the initial temperature with some displacement. Second, we assume that that we have no heat flowing in or out of the system, i.e., no additional heat transfer effects are considered. Thus, the temperature in the tubing can be expressed as the initial temperature with some displacement:

$$\boldsymbol{T(z,t) = T_i(z - vt)} \quad \text{A-1}$$

where $\boldsymbol{T}$ is the temperature in the tubing, $\boldsymbol{T_i(z)}$ is the initial temperature and the temperature change due to displacement is a function of the apparent displacement velocity $\boldsymbol{v}$ and time $\boldsymbol{t}$. Taking the time derivative of Eq. A-1 gives:

$$\frac{\partial T(z,t)}{\partial t} \approx \frac{T_i\,(z - v\Delta t) - T_i(z)}{\Delta t} \quad \text{A-2}$$

where $\frac{\partial T(z,t)}{\partial t}$ is the time derivative of the temperature response. Knowing that $\Delta z = v\Delta t$, Eq. A-2 can be rewritten as:

$$\frac{\partial T(z,t)}{\partial t} \approx v\,\frac{T_i(z - \Delta z) - T_i(z)}{\Delta z} \quad \text{A-3}$$

We then set the limit $\Delta z \to 0$:

$$\lim_{\Delta z \to 0} \frac{T_i(z - \Delta z) - T_i(z)}{\Delta z} = -\frac{\partial T_i\,(z)}{\partial z} \quad \text{A-4}$$

With this constraint, the time derivate of the temperature response is equivalent to the spatial derivative of the temperature response as a function of the displacement velocity:

$$= -v\,\frac{\partial T_i(z)}{\partial z} \approx \frac{\partial T(z,t)}{\partial t} \quad \text{A-5}$$

The initial temperature profile due to displacement of the fluid column can thus be expressed as:

$$T_i(z) = -\frac{1}{v}\int_{z_0}^{z} \frac{\partial T(z',t)}{\partial t}\, dz' + c \quad \text{A-6}$$

where $\boldsymbol{c}$ is a constant to get to absolute temperature values. In theory it is only required to have a single reference point (e.g., gauge measurement) to get the entire temperature profile displaying absolute temperature recordings from LF-DAS data. In this case, the time derivative of the temperature response is proportional to the LF-DAS data:

$$\frac{\partial T(z,t)}{\partial t} \propto \boldsymbol{DAS_{LF}(z,t)} \quad \text{A-7}$$